Ferroelectricity and weak ferromagnetism of hexagonal $ErFeO_3$ thin films

Hiroko Yokota,[1,*] Tomoya Nozue,[1] Shin Nakamura,[2,3] Hajime Hojo,[4] Mamoru Fukunaga,[5] Pierre-Eymeric Janolin,[6] Jean-Michel Kiat,[6,7] and Akio Fuwa[8]

[1]*Department of Physics, Chiba University, 1–33 Yayoi-cho, Inage-ku, Chiba-shi, Chiba 263–8522, Japan*

[2]*Department of Science and Engineering, Teikyo University, 1-1 Toyosatodai, Utsunomiya-shi, Tochigi 320–8551, Japan*

[3]*Advance Research Center of Science and Engineering, Waseda University, 3-4-1 Okubo, Shinjuku-ku, Tokyo 169–8555, Japan*

[4]*Materials and Structures Laboratory, Tokyo Institute of Technology 4259 Nagatsuta Midori-ku, Yokohama-City, Kanagawa 226–8503, Japan*

[5]*Department of Physics, Okayama University, 3-1-1, Tsushima-Naka, Kita-ku, Okayama 700–8530, Japan*

[6]*Laboratoire Structures, Propriétés et Modélisation des Solides, Université Paris Saclay, Centrale Supélec, CNRS; Grande voie des vignes, 92295 Châtenay-Malabry, France*

[7]*Laboratoire Léon -Brillouin, CE Saclay, 91191 Gif-sur-Yvette Cedex, France*

[8]*Department of Science and Engineering, Waseda University, 3-4-1 Okubo, Shinjuku-ku, Tokyo 169–8555, Japan*

(Received 7 May 2015; revised manuscript received 1 July 2015; published 3 August 2015)

Hexagonal $ErFeO_3$ thin films fabricated by a pulsed laser deposition method were investigated by x-ray diffraction (XRD) and transmission electron microscopy. No structural phase transition was observed between 20 and 900 K. Ferroelectric *D-E* hysteresis loops were obtained at room temperature using the double-wave method, and the magnitude of spontaneous polarization was determined to be 200 nC/cm^2. The existence of superlattice reflections in the XRD indicates that the space group of $ErFeO_3$ thin film is the polar hexagonal $P6_3cm$. This result also supports the ferroelectricity at room temperature. Magnetic properties were examined by a superconducting quantum interference device and Mössbauer spectroscopy. Below the Néel temperature of 120 K (T_N), a weak ferromagnetism appears along the *c* axis due to the canting of Fe^{3+} magnetic moments. Around T_N, the imaginary part of dielectric constant shows an anomaly. These results prove *h*-$ErFeO_3$ thin films to be multiferroic below 120 K.

DOI: 10.1103/PhysRevB.92.054101 PACS number(s): 77.80.−e, 68.55.−a, 81.15.Aa, 77.55.−g

I. INTRODUCTION

Multiferroics are the materials that possess more than two ferroic properties in the same phase [1]. Strong demands of energy-efficient devices for information storage promote extensive research on multiferroics, in particular, in the expectation of a strong coupling between ferroelectricity and magnetic order. It is well known that magnetic ions such as Fe, Co, Ni, and Mn located at the B site of perovskite oxides ABO_3 do not shift off-center to produce ferroelectricity because of their partially occupied *d* orbitals [2]. This fact has been considered to be the origin of the scarcity of multiferroic materials. In the past few decades, however, other kinds of scenarios avoiding the aforementioned difficulty have been devised to realize multiferroicity. One direction is so called type II multiferroics [3]. In this class, a strong magnetoelectric coupling has been reported since ferroelectricity is induced by magnetic ordering [4–6]. However, ferroelectric phase transition normally takes place at low temperature, and the magnitude of spontaneous polarization is rather small. The hexagonal (*h*) rare earth (*R*) manganites, $RMnO_3$, represent another scenario. In fact, the first report on the possibility of multiferroicity goes back to the 1960s [7–17]. *h*-$RMnO_3$ possesses a rather particular structure as ABO_3 forms [13]. It exhibits a dense oxygen-ion packing, with Mn^{3+} having a coordination number of five to form corner-linked fivefold trigonal bipyramids in the (001) plane. R^{3+} ions with seven coordination numbers are in capped octahedra, which separate MnO_5 layers along the polar [001] direction. Ferroelectricity appears as a result of the buckling of oxygen bipyramid accompanied by the shift of *R* ions, and the antiferromagnetic order of Mn^{3+} ions arises from the Mn-O-Mn superexchange interaction.

Contrary to the fact that a lot of studies have been performed on *h*-$RMnO_3$, the research on hexagonal *R* ferrites (*h*-$RFeO_3$) has been limited [18–31]. The main reason for this is the difficulty of synthetizing $RFeO_3$ in the hexagonal form since $RFeO_3$ is apt to be orthorhombic with a centrosymmetric space group, which does not permit ferroelectricity [32,33]. However *h*-$RFeO_3$ with R = Eu-Lu was synthesized in thin film form using the metal organic chemical vapor deposition (MOCVD) technique on yttria stabilized zirconia (YSZ) substrates [16]. The ferroelectricity and magnetic orders were first reported for *h*-$YbFeO_3$ films synthesized by the pulsed laser deposition (PLD) method on YSZ substrates, and ferroelectric and ferrimagnetic transition temperatures were determined to be 350 and 100 K, respectively, by exploiting dielectric measurements, optical second harmonic generation (SHG), x-ray diffraction (XRD), and a superconducting quantum interference device magnetometer (SQUID) [22,24]. Until now, *h*-$RFeO_3$ films with various R(=Yb, Lu, Er, and Ho) and $InFeO_3$ film have been synthesized by the MOCVD or the PLD technique, and their multiferroicity was examined upon some of those films [20,22–31].

The recent first-principle calculations on the *h*-$RFeO_3$ system figured that with decreasing the radius of *R* ions, the electric polarization is enhanced, and a weak ferromagnetism is induced along the *c* axis [34,35]. In the present study, we focus on *h*-$ErFeO_3$, which is expected to show a robust multiferroicity. Previous experimental papers, though they are scarce, found an anomaly in the optical absorption due to the magnetic ordering of Fe sublattice at 124 K [28] and determined atomic shifts of Er ions relative to FeO_5

*Email address: hiroko.9bq@chiba-u.jp

using an aberration-corrected scanning transmission electron microscope (STEM) from which a remnant polarization was evaluated to be 8.1 $\mu C/cm^2$ at room temperature [30].

Considering the aforementioned situation, it seems to us that there still exists a necessity of more direct evidences of ferroelectric and magnetic properties of h-$R$$FeO_3$ in order to understand multiferroic h-$R$$FeO_3$. In the present paper, we synthesized h-$ErFeO_3$ films using the PLD method; examined the crystal structure by XRD and a transmission electron microscope (TEM); measured the dielectric constant, the D-E hysteresis, and the superlattice reflections to confirm the ferroelectricity; and applied the SQUID and the Mössbauer spectroscopy to determine the magnetic structure. The Mössbauer spectroscopy is a powerful technique to obtain the information on the magnetic structure and the electronic state. It provides the isomer shift, the quadrupole splitting, and the hyperfine field, which determine the valence of Fe ions, local structure, and magnetic structure, respectively. In combination with the SQUID analysis, we successfully identified the magnetic ordering in h-$ErFeO_3$ thin film.

II. EXPERIMENT

A. Thin film fabrications and structural characterizations

Hexagonal $ErFeO_3$ thin films were fabricated using a PLD method with the fourth harmonics of Nd:YAG laser ($\lambda = 266$ nm). Orthorhombic $ErFeO_3$ ceramics were used as targets, and thin films were grown on YSZ (111) ($a = 5.16$ Å, lattice misfit -3%) and α-Al_2O_3 (0001) ($a = 4.76$ Å, $c = 12.99$ Å, lattice misfit -0.2%) substrates. Optimized fabrication conditions were an oxygen pressure of 300 mTorr and a substrate temperature of 850 °C. The obtained thin films were examined by the XRD with Cu source (using Kα_1 wavelength) under different configurations (θ-2θ scan, ϕ scan, and asymmetric θ-2ω scan). The morphology of the $ErFeO_3$ thin films was examined by atomic force microscope (AFM), and a smooth surface with the root mean square (RMS) of 0.345 nm was confirmed. High-resolution TEM (HRTEM) images and selected-area electron diffraction (SAED) patterns were taken along the $[1\bar{1}0]$ direction of the YSZ substrate using a JEOL JEM-2100F microscope. The sample for TEM observations was prepared by mechanically polishing to a thickness of about 10 μm followed by Ar-ion milling so that the electron transparency could be obtained.

In order to examine the structural phase transition, XRD measurements were carried out by a highly accurate, two-axis diffractometer with the Bragg-Brentano geometry issued from a Rigaku rotating anode using a Cu Kα_1 wavelength over a wide temperature range from 20 to 873 K. The lattice constants of the h-$ErFeO_3$ thin film at room temperature were refined from 000l reflections ($l = 2,4,6,8$) in order to correct for possible misalignments and serve as a reference. The lattice parameter evolution with temperature was determined from the 0002 reflection at low temperature and the 0001 reflection at high temperature. The XRD profiles were analyzed with the pseudo-Voigt function. The lattice constants of the YSZ substrate were also measured as a reference at each temperature.

B. Dielectric measurements

For the dielectric measurement, an indium tin oxide (ITO) thin film was deposited by the PLD method as a bottom electrode, and Au was evaporated as a top electrode. The complex dielectric constants of the h-$ErFeO_3$ thin film were measured as a function of temperature using an impedance analyzer (Keysight Technologies E4990A) equipped with a closed-cycle refrigerator.

The electric resistivity of the h-$ErFeO_3$ thin film along the c axis was measured using a source meter (Keithley 2400) at room temperature. Because of rather high electric conductivity of the $ErFeO_3$ films, special care was paid for measuring D-E hystereses. For this purpose, we adopted the double wave method (DWM) to determine the remnant polarization at room temperature [36]. Sinusoidal wave was applied along the c axis of the h-$ErFeO_3$ thin film with the changing of the amplitude of the voltage. The frequency of the sinusoidal wave was fixed at 30 Hz. Using this technique, the conductive component can be separated from the loop, and a reliable D-E hysteresis loop can be obtained.

C. Magnetic properties

Static magnetic properties of the h-$ErFeO_3$ thin film were examined with the SQUID (Quantum Design MPMS). A magnetic field was applied either perpendicular (out-of-plane: $H \parallel c$) or parallel (in-plane: $H \perp c$) to the thin film. Temperature dependences of magnetizations were measured under magnetic fields of different magnitudes. Magnetic hysteresis measurements were performed at several temperatures under the out-of-plane configuration.

Mössbauer spectra were measured in the conventional transmission geometry using a ^{57}Co-in Rh (25 mCi) as the γ-ray source. The incident direction of γ-ray was parallel to the c axis of $ErFeO_3$ thin film within the accuracy of $\pm 5^\circ$. The Doppler velocity scale was calibrated with an Fe metal foil measured at room temperature. Since the natural abundance of Mössbauer active ^{57}Fe is only 2.2% and it makes the Mössbauer measurements difficult to perform on thin films, we used 100% ^{57}Fe as a starting material and fabricated ^{57}Fe-enriched $ErFeO_3$ thin film, which allowed us to carry out the Mössbauer experiments. The ^{57}Fe-enriched $ErFeO_3$ thin film deposited on the Al_2O_3 (0001) substrate was used as a specimen since the YSZ substrate exhibits a strong absorption effect. XRD and SQUID experiments conducted on the ^{57}Fe-enriched $ErFeO_3$ thin film on Al_2O_3 (0001) substrate showed the same qualities with that of the thin film deposited on the YSZ substrate. Mössbauer spectra were collected at several temperatures using liquid nitrogen or helium cryostats and a closed cycle refrigerator. The absorption line shapes were assumed as the Lorentzian function. A precise combination of magnetic and quadrupole Hamiltonians was used for the spectra analysis obtained below the magnetic phase transition temperature.

III. EXPERIMENT RESULTS

A. Structural characterizations

Figure 1(a) shows the XRD profile of $ErFeO_3$ thin film fabricated on a YSZ (111) substrate. Only 000l reflections of

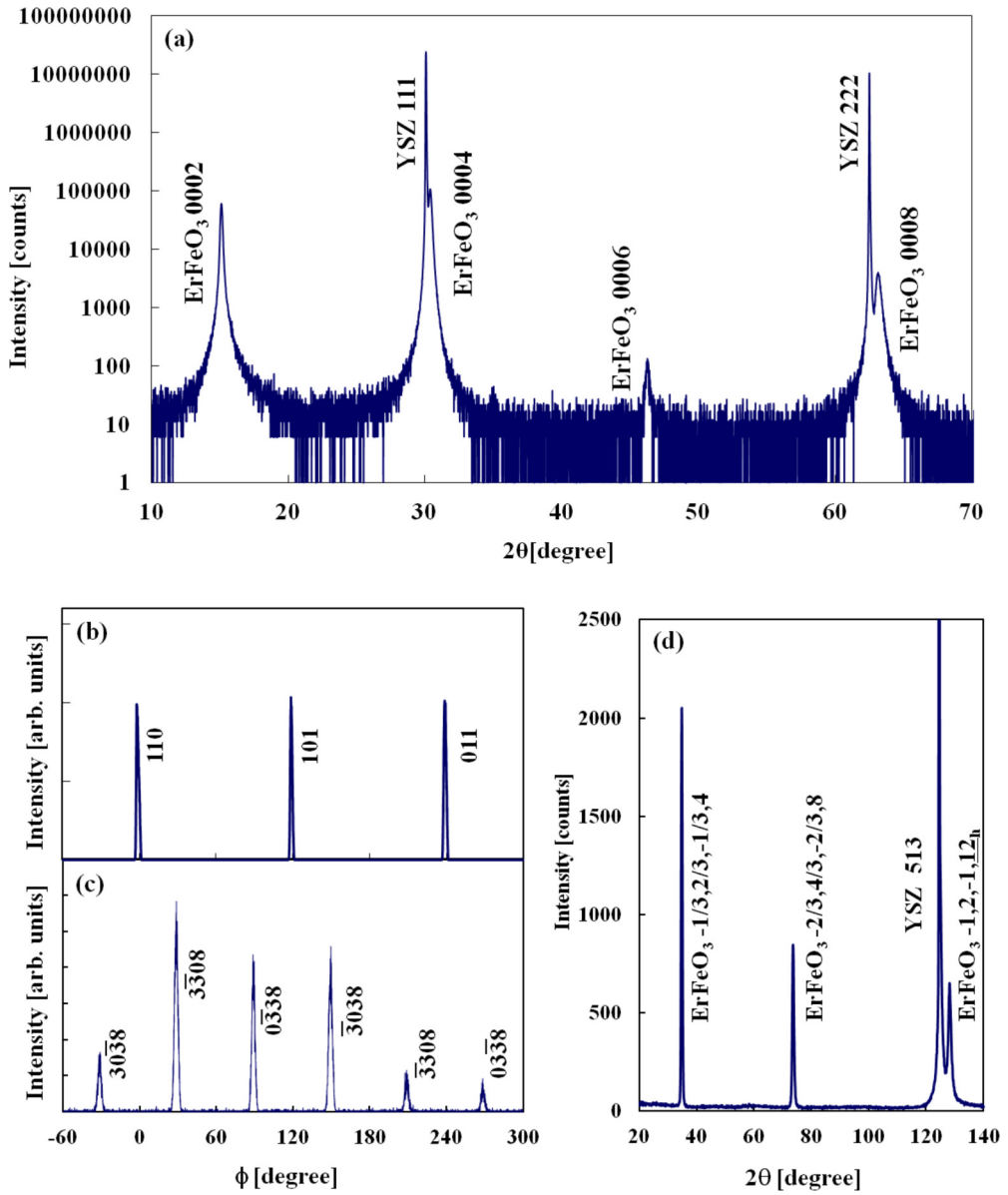

FIG. 1. (Color online) XRD profiles of the h-$ErFeO_3$ thin film deposited on the YSZ (111) substrate. (a) $\theta - 2\theta$ profile showing the [0001] oriented growth; (b) and (c) correspond to the ϕ scan of YSZ 110 and the h-$ErFeO_3$ $30\bar{3}8$ reflections, respectively. (d) The $\theta - 2\omega$ profile of the h-$ErFeO_3$ thin film. Two superlattice reflections of the $ErFeO_3$ thin film are observed around 35° and 74° together with main reflections from h-$ErFeO_3$ and the YSZ substrate.

the hexagonal $ErFeO_3$ thin film and YSZ hhh reflections are observed, and no impurity or secondary phases are detected. It indicates that the obtained thin film is c axis oriented. We also examined the h-$ErFeO_3$ thin film deposited on an Al_2O_3 (0001) substrate and confirmed that the obtained thin film is also c axis oriented without any impurity phases. The c axis lattice parameter of thin film is obtained as 11.770 Å at room temperature. The rocking curve of the 0008 peak has the full-width at half maximum (FWHM) of 0.2°. Figure 1(b) illustrates the ϕ scan profile of the YSZ 110 reflections. Three peaks with 120° separation prove the existence of the threefold axis along the [111] direction of the YSZ substrate. In Fig. 1(c), six peaks corresponding to the h-$ErFeO_3$ 308 reflections appear every 60°, which are 30° apart from those of the YSZ substrate. It demonstrates that the h-$ErFeO_3$ thin film is epitaxially grown on the YSZ (111) substrate and that the $[1\bar{1}00]$ orientation of the $ErFeO_3$ thin film is parallel to the $[1\bar{1}0]$ YSZ substrate. The result of the asymmetric scan around the 513 reflection of the YSZ substrate is shown in Fig. 1(d). Two superlattice peaks corresponding to $-1/3\,2/3\ -1/3\,4_h$ and $-2/3\,4/3\ -2/3\,8_h$ reflections are detected in addition to the $-1\,2\ -1\,12_h$ main reflection. The observation of these superlattice reflections indicates that the space group of the $ErFeO_3$ thin film is polar $P6_3cm$, which permits ferroelectricity. Figure 2(a) exhibits the HRTEM image of the h-$ErFeO_3$ thin film. The right part corresponds to the YSZ substrate, and the left area is the thin film. The cross section image reveals that no amorphous layer or domain boundary exists in the thin film. The SAED pattern shown in Fig. 2(b) indicates that the epitaxial relationship

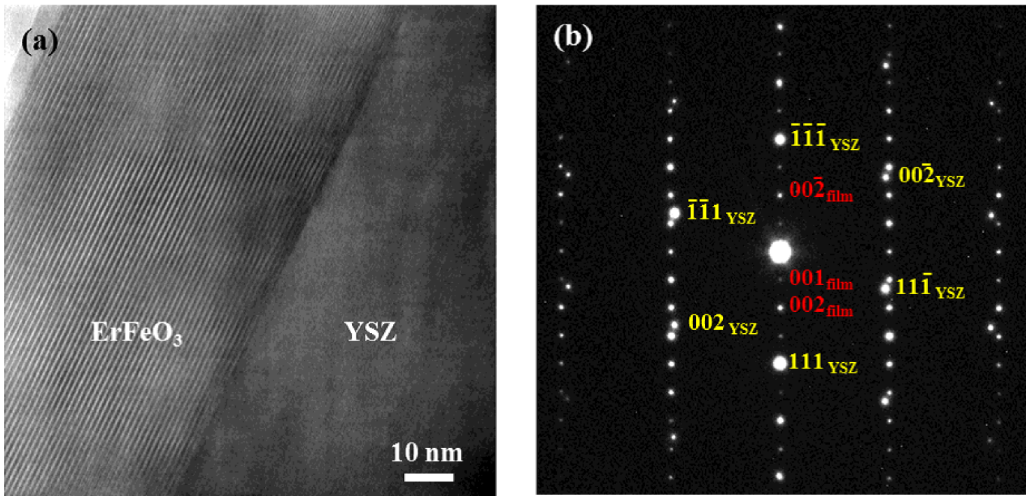

FIG. 2. (Color online) (a) HRTEM image of the h-$ErFeO_3$ thin film deposited on the YSZ substrate. No amorphous phase is observed at the interface between the h-$ErFeO_3$ thin film and YSZ substrate, as observed in the h-$YbFeO_3$ thin films [24]. (b) SAED pattern of the h-$ErFeO_3$ thin film, showing that the thin film is c axis oriented.

between the $ErFeO_3$ thin film and the YSZ substrate coincides well with XRD results.

Figures 3(a) and 3(b) show the temperature dependences of lattice constants measured in low and high temperatures, respectively. Lattice constants of the YSZ substrate and the h-$ErFeO_3$ thin film increase monotonically with increasing temperature, and no anomaly corresponding to a structural phase transition is observed within experimental errors. This result could be evidence that the h-$ErFeO_3$ film does not show ferroelectric to paraelectric phase transition at least until 900 K, which is accompanied by clear spontaneous strains, as observed in h-$REMnO_3$ compounds [37,38].

B. Dielectric properties

Temperature dependences of real (ε') and imaginary (ε'') parts of the dielectric constant measured at 10 kHz are depicted in Fig. 4(a). ε' is around 45 at 300 K, which is comparable with the reported value of the h-$YbFeO_3$ thin film [24]. ε' decreases monotonically with cooling the specimen, and no anomalies corresponding to the phase transition are observed. On the other hand, ε'' shows an anomaly around 140 K, which is close to the magnetic transition temperature that will be discussed later. Thus, it would suggest the possibility of magnetoelectric coupling in the h-$ErFeO_3$ thin film. The magnitude of the dielectric loss ($\tan\delta = \varepsilon''/\varepsilon'$) is less than 0.01 at room temperature. This value is rather small among multiferroics but is still one order of magnitude larger than classical ferroelectrics. The electric resistivity of the h-$ErFeO_3$ thin film is around 10^8 Ωcm at room temperature, as shown in Fig. 4(b).

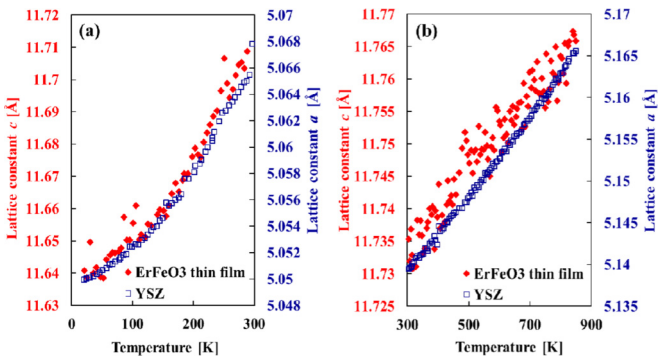

FIG. 3. (Color online) Temperature dependences of lattice constants of the h-$ErFeO_3$ thin film and YSZ substrate. (a) Result in the low temperature and (b) in the high temperature. Red solid diamonds indicate the h-$ErFeO_3$ lattice constant, and blue open squares indicate the YSZ lattice constant. Left axis corresponds to the h-$ErFeO_3$ lattice constant and right axis to that of YSZ. No anomaly corresponding to the structural phase transition is observed in this temperature range within the experimental error.

Figure 4(c) exhibits the D-E hysteresis loop measured at room temperature. We carried out the experiments with changing the amplitude of the electric field and confirmed that the magnitude of spontaneous polarization shows almost the same value. The asymmetric form of the loops shows the existence of internal bias field in the thin film, supposedly originated from the asymmetric configuration electrodes. The spontaneous polarization P_S is estimated to be 200 nC/cm^2, which is much smaller than the predicted value from the first principle calculations [35] of 8.3 $\mu C/cm^2$ and the point charge model based on crystal structure of 9 $\mu C/cm^2$ [30]. The origin of the discrepancy is not clear at present. We believe that it is caused by the existence of nonswitchable parts in our thin films, but further experiments by TEM and D-E hysteresis measurements on the same specimen are awaited for clarifying this point.

C. Magnetic properties

1. *Superconducting quantum interference device*

Figure 5(a) describes the out-of-plane temperature hysteresis of magnetization under the magnetic field of 100 Oe. It is found that the magnetic susceptibility obeys the Curie-Weiss law above 200 K, which is much higher than the magnetic transition temperature of $T_N = 120$ K. At 120 K, a magnetic

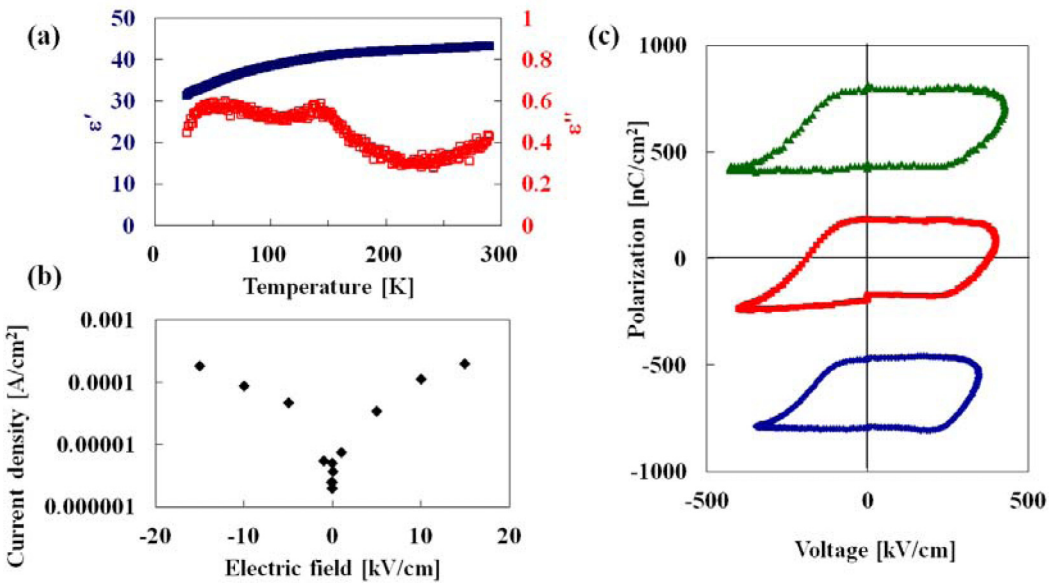

FIG. 4. (Color online) (a) Temperature dependences of the dielectric constant of the h-$ErFeO_3$ thin film measured at 10 kHz. Blue solid and red open squares correspond to the real (ε') and imaginary part (ε'') of the dielectric constant, respectively. ε' is graphed against the y axis scale on the left edge of the graph and ε'' on the right edge. ε'' exhibits a hump around 140 K. (b) Resistivity of the h-$ErFeO_3$ thin film at room temperature. (c) D-E hysteresis loops of the $ErFeO_3$ thin film measured at room temperature under different amplitudes of the electric field. The magnitude of spontaneous polarization is estimated to be around 200 nC/cm^2. The asymmetric form of the loops shows the existence of internal field in the thin film.

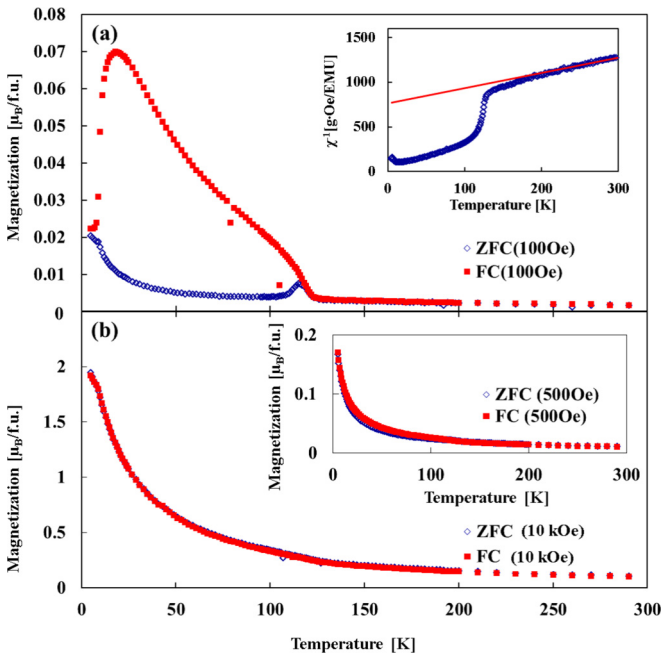

FIG. 5. (Color online) Temperature dependence of the magnetization of the h-$ErFeO_3$ thin film. The magnetic field is applied parallel to the c axis of the h-$ErFeO_3$ thin film for (a) and (b). In the inset graph of (b), the magnetic field (500 Oe) is applied perpendicular to the c axis. The magnitudes of the magnetic field are 100 Oe and 10 kOe for (a) and (b), respectively. Blue open diamonds represent the ZFC process, and red solid squares correspond to the FC process. The inverse susceptibility is shown as an inset in (a). It obeys the Curie-Weiss law above 200 K.

transition takes place with different paths between zero-field cooling (ZFC) and field cooling (FC) processes observed in the out-of-plane configuration. In the ZFC process, the magnetization shows a small peak at 115 K, and it increases monotonically with a decrease of the temperature. In the FC process, magnetization also increases but suddenly drops around 18 K and then turns to increase again at 5 K. In Fig. 5(b), the result of temperature dependence of magnetization under a magnetic field of 10 kOe is summarized. In contrast with the case of smaller magnetic field, the temperature hysteresis disappears, and magnetization increases monotonically with decreasing temperature. This result indicates that the drop of magnetization observed below 18 K under the low magnetic field is caused by the increase of magnetic anisotropy. The inset of Fig. 5(b) describes the temperature dependence of magnetization in the in-plane configuration. Under 500 Oe, a clear temperature hysteresis does not exist, and ZFC and FC processes exhibit almost similar behavior. The results of the magnetic hysteresis measurements are summarized in Fig. 6. Below 120 K, apparent hysteresis loops are observed, but they do not saturate up to 50 kOe. With a decrease of the temperature, the remnant magnetization increases. The magnetic hysteresis measurement was also conducted under the in-plane configuration, and it does not exhibit a hysteresis loop, which is characteristic for the weak ferromagnetics.

2. *Mössbauer spectroscopy*

Figure 7 describes the Mössbauer spectrum measured at several temperatures. Paramagnetic spectrum consisting of an asymmetric doublet is observed at 291 K, as shown in Fig. 7(a). The isomer shift and the quadrupole splitting are

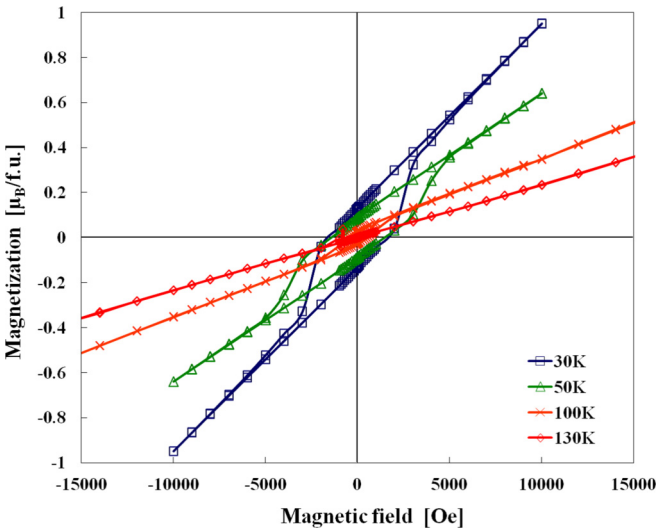

FIG. 6. (Color online) Magnetic hysteresis loops measured at 30 K (blue square), 50 K (green triangle), 100 K (orange cross), and 130 K (red diamond). The magnetic field is applied parallel to the c axis of the h-$ErFeO_3$ thin film. Hysteresis loops are observed at 30, 50, and 100 K.

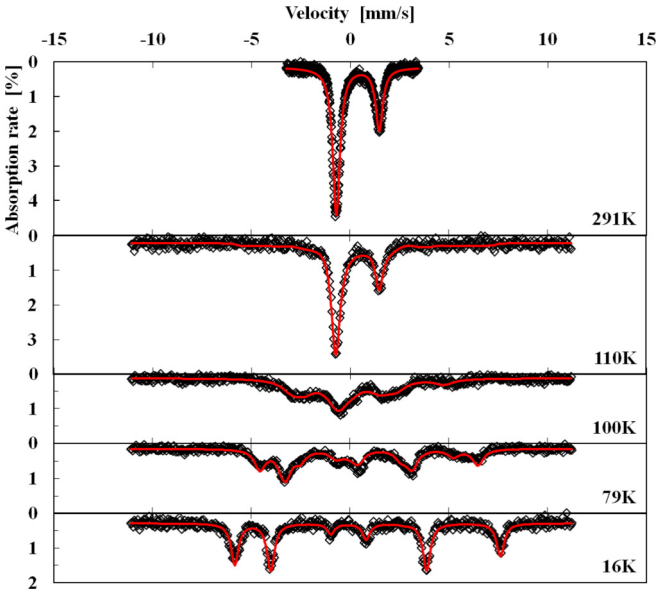

FIG. 7. (Color online) Mössbauer spectra measured at (a) 291, (b) 110, (c) 100, (d) 79, and (e) 16 K. Open diamonds represent the experimental data, and the solid red line corresponds to the fitting result.

0.299 and -2.12 mm/s, respectively. The value of the isomer shift suggests that the Fe ions are in a high-spin Fe^{3+} state. A relatively high value of quadrupole splitting shows that the Fe ion locates in a low symmetry site, and this result coincides well with a distorted pentahedral oxygen coordination [13], which also supports the ferroelectricity of h-$ErFeO_3$ at room temperature. The FWHM of the spectrum is relatively large at 0.423 mm/s, which implies that the oxygen bipyramid is inhomogeneous, and it might cause a rather small spontaneous polarization. Mössbauer spectra start to change at 120 K, and it cannot be explained with a simple paramagnetic spectrum at 110 K, shown in Fig. 7(b). Below 100 K, drastic changes can be observed in Figs. 7(c) and 7(d). At 16 K, a well-resolved magnetically ordered spectrum is obtained, as described in Fig. 7(e). It is clearly seen that the second and fifth absorption lines ($\Delta m_I = 0$ transition) have stronger intensities, which indicates that the hyperfine field (or magnetic moment) lies approximately in the ab plane, i.e., in the plane of the film.

In order to analyze the spectra precisely, here we calculate the principal axes of the electric field gradient (EFG) for the Fe site, assuming a point charge model for the electric potential. Since no crystal structural data of h-$ErFeO_3$ exist, structural parameters of h-$RMnO_3$ measured at room temperature were adopted for the calculation [39]. The EFG tensor component at the Fe site can be calculated using

$$V_{pq} = \sum_{i}^{\text{lattice}} \frac{\partial^2}{\partial p \partial q} V^{(i)}. \quad (1)$$

Here, p and q denote the orthogonal axes (x,y,z), and $V^{(i)}$ expresses the electric potential by the ith element. The obtained tensor is diagonalized to provide the principle axes of the EFG. The calculated EFG axes at room temperature are illustrated in Fig. 8. The x axis of EFG is perpendicular to the crystallographic a and c axes. The y and z axes are in the ac plane and are inclined at around 13° from the hexagonal c axis.

We also calculated the quadrupole coupling constant $e^2qQ/2$ and asymmetry parameter η, and they are -1.5 mm/s and 0.1, respectively, at room temperature. The calculated $e^2qQ/2$ value is smaller than the experimental result of -2.119 mm/s (assuming $\eta = 0.1$). This discrepancy might be caused by the oxygen-dipole effect and/or the spin-orbital interaction. The important point is that the calculated $e^2qQ/2$ exhibits a good agreement, although the h-$RMnO_3$ crystal structural parameters are used. To further examine the validity of the EFG axes, the intensity ratio of the paramagnetic spectrum is calculated using the obtained angles between the EFG axes and the incident γ ray direction. The calculated $I(\pm 3/2)/I(\pm 1/2)$ is 2.70, which is rather close to the experimentally obtained ratio of $I_1/I_2 = 2.40$. This result indicates that the obtained principle axes of the EFG are appropriate. Then the magnetic spectra at low temperature were analyzed with respect to the calculated EFG axes. The obtained Mössbauer parameters, i.e., the isomer shift, $e^2qQ/2$, the hyperfine field (H_{hf}), and the line width, are summarized as a function of temperature in Fig. 9. As shown in Fig. 9(a), the isomer shift continuously increases towards low temperature. Note that the spectra around 100 K, just below T_{N}, are complex and analyzed as the composition of two subspectra, which may cause larger errors in the isomer shift at this temperature range. The increase of isomer shift with decreasing temperature is consistent with the fact that the effect of lattice vibration becomes weaker and closer to the chemical shift of Fe^{3+} at 0 K. Meanwhile, the isomer shift at 4.2 K (0.396 mm/s) takes a slightly smaller value than the typical Fe^{3+} value. Figure 9(a) describes the temperature dependence of $e^2qQ/2$. $e^2qQ/2$ is almost temperature independent, which is typical for the Fe^{3+} state. H_{hf} appears below the magnetic transition temperature and obeys the Brillouin function [Fig. 9(b)]. The magnitude of H_{hf} at 4.2 K is 412 kOe, which is much smaller than the normal

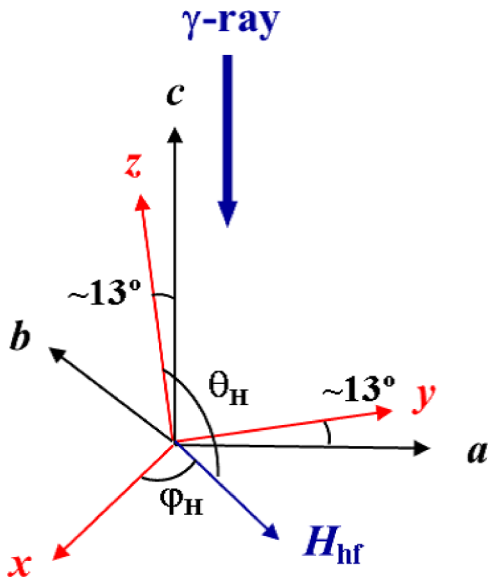

FIG. 8. (Color online) The relationship between the crystallographic axes (abc), the EFG axes (xyz), and the hyperfine field $H_{\rm hf}$. The incident direction of γ ray is parallel to the c axis. θ_H and φ_H are the Euler angles of the hyperfine filed with respect to the principle axis of the EFG.

Fe^{3+}. The line width exhibits an anomaly around the magnetic transition temperature, shown in Fig. 9(b).

IV. DISCUSSION

A. Electronic state

According to the results of the Mössbauer spectroscopy, Fe ions of the h-$ErFeO_3$ thin film are basically the high spin state of Fe^{3+}. However, as we mentioned in the previous section, the isomer shift at 4.2 K is smaller than the typical Fe^{3+} value of 0.45−0.50 mm/s. It denotes that the electron density at the Fe site is slightly low. Additionally, the hyperfine field shows a rather smaller value of 412 kOe than the ordinary Fe^{3+} value of 500−550 kOe. A smaller value of $H_{\rm hf}$ was reported in the RFe_2O_4 family crystals that possess fivefold trigonal bipyramids, as in h-$ErFeO_3$ [40,41]. However, $H_{\rm hf}$ of RFe_2O_4 is around 470 kOe. Therefore, a lower symmetry of the Fe^{3+} site is not enough to explain such a small $H_{\rm hf}$ value in the h-$ErFeO_3$ thin films. We evaluate the magnetic moment to be 3.75 μ_B assuming that the hyperfine coupling constant A is 110 kOe/μ_B. The evaluated value is much smaller than the spin only value of 5 μ_B. A similar phenomena has been observed in iron sulfides, which possess high covalent bondings [42,43]. Thus, it is expected that the Fe 3d and O 2p orbitals are partially covalent, and delocalization of 3d electron occurs in the h-$ErFeO_3$ thin film. This is consistent with our experimental results of low dielectric constant and small spontaneous polarization. The observation of covalent bond formations in the Fe-O bonds in the h-$LuFeO_3$ powder obtained by high-energy synchrotron-radiation experiments also supports our experimental results [21]. In order to make clear the electronic state of the Er ion, we are planning to carry out the x-ray magnetic dichroism (XMCD).

B. Magnetic structure analysis

As shown in Fig. 6, the h-$ErFeO_3$ thin film shows magnetic hysteresis below T_N. Nevertheless, the magnetic moment does not saturate even at 5 T and increases linearly under a large magnetic field. In the h-$ErFeO_3$ system, we have two magnetic ions (Er and Fe), and it makes the magnetic structure complicated. Figure 10 shows the hysteresis loops after subtracting the linear component χH at different temperatures. It exhibits a well-saturated hysteresis loop, indicating weak ferromagnetism below T_N. The remnant magnetization increases towards low temperature and becomes around 0.15 μ_B/f.u. at 30 K. If we assume that the spontaneous magnetization mainly originates from Fe^{3+} ions having a magnetic moment of 5 μ_B, the canting angle from the ab plane can be estimated to be 1.7°. Since the magnitude of spontaneous magnetization at lower temperature cannot be estimated due to the strong anisotropy, a slightly larger canting angle would be expected at a much lower temperature. The estimated canting angle is the typical value for weak ferromagnetism.

Hereafter, we discuss the magnetic structure of the Fe ion by considering the direction of the hyperfine field in Mössbauer spectrum at low temperature. The Euler angles $(\theta_H,\varphi_H) = (95(5),30(10)^\circ)$ provides the best fit for the Mössbauer

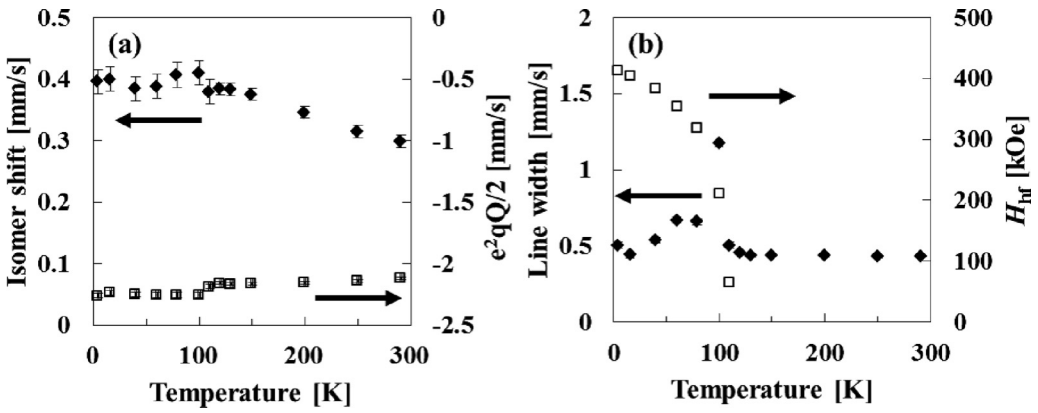

FIG. 9. The Mössbauer parameters as a function of temperature. The isomer shift (solid diamond) and quadrupole coupling constant (open square) are shown in (a). The y axis scale of the isomer shift and quadrupole coupling constant are on the left and right side of the graph, respectively. (b) Line width (solid diamond) and hyperfine field (open square); scales are on the left and right edge of the graph, respectively.

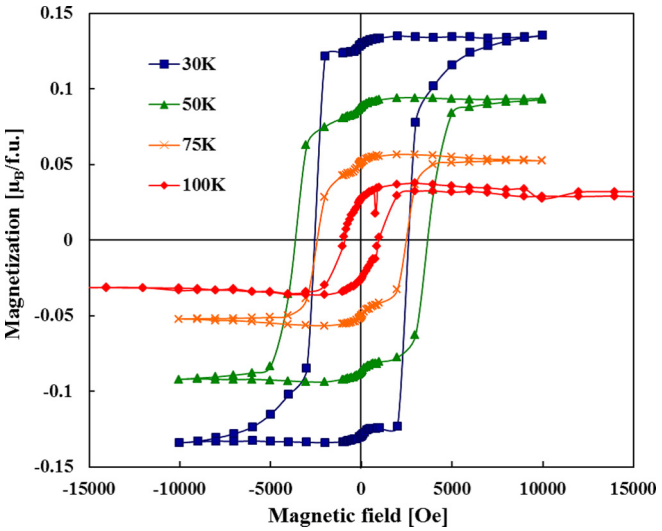

FIG. 10. (Color online) Magnetic hysteresis loops at several temperatures after subtracting the linear component χH. Red diamonds correspond to 100 K, orange crosses to 75 K, green triangles to 50 K, and blue squares to 30 K, respectively. They exhibit ferromagnetic behaviors at this temperature range.

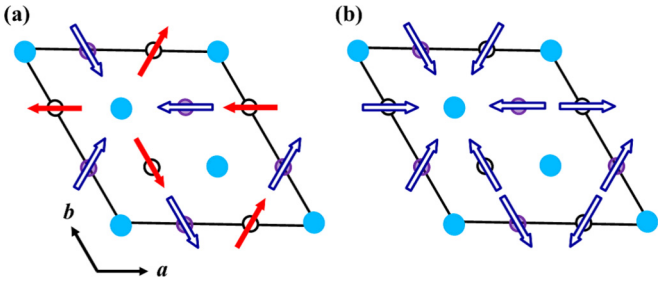

FIG. 11. (Color online) The possible spin configurations of the Fe^{3+} site. Large solid circles represent the Er ion. Small open circles and solid circles represent the Fe ion at $c = z$ and $c = z + 1/2$ sites, respectively. The arrow indicates the direction of the magnetic moment. The open arrow is canted from the ab plane towards the $+c$ axis, and the solid arrow represents the canting towards the $-c$ axis. (a) The α model with $\varphi = 0°$; (b) the β model with $\varphi = 0°$ [37,38].

spectrum. Here, the Euler angles are defined as the orientation of the hyperfine field (or the magnetic moment) with respect to the principal axes of the EFG. The relationship between the orientation of the hyperfine field and the EFG is illustrated in Fig. 8. Since the Mössbauer measurement cannot distinguish θ_H and $180° - \theta_H$, the direction of magnetic moment is inclined either $\pm 10(5)$ or $\pm 20(5)°$ from the ab plane. The direction of the magnetic moment in the ab plane is determined as approximately parallel to $-b$ direction from $\varphi_H = 30(10)°$. With the consideration of crystal symmetry, the magnetic moment on the same c plane has an almost triangular lattice structure. We assume that the magnetic unit cell takes the structure of the crystallographic unit cell, and we only consider the nearest neighbor interaction. The Dzialoshinskii-Moriya (DM) interaction is one of the possible origins to cant the magnetic moment in h-$ErFeO_3$. The existence of the DM interaction is determined by the symmetry, and the direction of the DM vector $\boldsymbol{d}$ follows five rules. Among them, the h-$ErFeO_3$ system satisfies two rules. As an intralayer interaction, $\boldsymbol{d}$ lies in the {110} mirror plane. For an interlayer interaction, $\boldsymbol{d}$ is perpendicular to the {100} mirror plane. Taking into account the large separation between the adjacent layers, the intralayer interaction is dominant, and it would induce weak ferromagnetism in h-$ErFeO_3$ along the c axis. Consequently, the possible spin configurations of Fe ions based on Mössbauer spectroscopy are described in Fig. 11. As shown in Fig. 11(a), the spins at different c positions are canted in opposite directions from the ab plane. Therefore, the total magnetic moment is cancelled, and it exhibits antiferromagnetism. On the other hand, all spins align in the same direction from the ab plane and shows weak ferromagnetism, as illustrated in Fig. 11(b). Combining the fact that the $ErFeO_3$ thin film exhibits magnetic hysteresis below T_N, antiferromagnetic configurations are safely eliminated, and the weak ferromagnetic structure of Fig. 11(b) is the most probable candidate to represent the spin configuration of h-$ErFeO_3$ thin film. These two structures correspond to the α and β models, with $\varphi = 0°$ [44,45]. Here the α model does not allow the ferromagnetism, but the β model permits it. It is interesting that h-$RFeO_3$ belongs to the β model, while all h-$RMnO_3$ belong to the α model [46,47]. Since the Mössbauer experiment contains an approximately $\pm 5°$ error on the angle due to the sample setting, the canting angle obtained from the Mössbauer spectra shows a good agreement with the result of magnetic hysteresis loop. However, further investigations are still needed to understand the behavior of magnetic hysteresis loop, and we are planning to perform the SQUID experiments under higher magnetic fields and the Mössbauer spectroscopy under a magnetic field.

V. CONCLUSIONS

We demonstrated that hexagonal $ErFeO_3$ thin films fabricated by the PLD method are epitaxially grown on YSZ (111) substrates in a single phase. No clear structural phase transition was observed between 20 and 900 K. Ferroelectricity of the h-$ErFeO_3$ thin film is clarified by the existence of superlattice reflections and the D-E hysteresis measurements with the DW technique at room temperature. The magnitude of the spontaneous polarization is 200 nC/cm^2 at room temperature. The imaginary part of the dielectric constant shows a definite anomaly around the magnetic transition temperature of 120 K. The SQUID measurements reveal that weak ferromagnetism originating from the Fe canting magnetic moment appears below the magnetic transition temperature. These results show that ferroelectricity and weak ferromagnetism coexist in the h-$ErFeO_3$ thin film below 120 K, and h-$ErFeO_3$ films are multiferroics. The Mössbauer spectroscopy discloses that the Fe ions are in the high-spin Fe^{3+} state and are located in the distorted pentahedral oxygen coordination. It also confirms the appearance of weak ferromagnetism accompanied by Fe canting due to the DM interaction. The possibility of hybridization between Fe $3d$ and O $2p$ orbital is pointed out.

ACKNOWLEDGMENTS

H.Y. acknowledges the support by Grant-in-Aid for Young Scientists (B) (Grant No. 24740195) from the Ministry of Education, Culture, Sports, Science and Technology, Japan, and the research grant (Grant No. 0261011-A) from Iketani Science and Technology Foundation, Japan. The authors are grateful to Kay Kohn and Yoshiaki Uesu for insightful discussions and critical reading of the manuscript.

[1] H. Schmid, Ferroelectrics **162**, 317 (1994).
[2] N. A. Hill, J. Phys. Chem. B **104**, 6694 (2000).
[3] D. Khomskii, Physics **2**, 20 (2009).
[4] T. Kimura, T. Goto, H. Shintani, K. Ishizaka, T. Arima, and Y. Tokura, Nature **426**, 55 (2003).
[5] T. Goto, T. Kimura, G. Lawes, A. P. Ramirez, and Y. Tokura, Phys. Rev. Lett. **92**, 257201 (2004).
[6] T. Kimura, G. Lawes, T. Goto, Y. Tokura, and A. P. Ramirez, Phys. Rev. B **71**, 224425 (2005).
[7] E. F. Bertaut and M. Mercier, Phys. Lett. **5**, 27 (1963).
[8] N. Fujimura, T. Ishida, T. Yoshimura, and T. Ito, Appl. Phys. Lett. **69**, 1011 (1996).
[9] Z. J. Huang, Y. Cao, Y. Y. Sun, Y. Y. Xue, and C. W. Chu, Phys. Rev. B **56**, 2623 (1997).
[10] A. Muñóz, J. A. Alonso, M. J. Martínez-Lope, M. T. Casáis, J. L. Martínez, and M. T. Fernández-Díaz, Phys. Rev. B **62**, 9498 (2000).
[11] M. Fiebig, T. Lottermoser, D. Fröhlich, A. V. Goltsev, and R. V. Pisarev, Nature **419**, 818 (2002).
[12] H. Sugie, N. Iwata, and K. Kohn, J. Phys. Soc. Jpn. **71**, 1558 (2002).
[13] B. B. van Aken, T. T. M. Palstra, A. Filippetti, and N. A. Spaldin, Nature Mater. **3**, 164 (2004).
[14] T. Lottermoser, T. Lonkai, U. Amann, D. Hohlwein, J. Ihringer, and M. Fiebig, Nature **430**, 541 (2004).
[15] B. Lorenz, Y. Q. Wang, Y. Y. Sun, and C. W. Chu, Phys. Rev. B **70**, 212412 (2004).
[16] O. P. Vajk, M. Kenzelmann, J. W. Lynn, S. B. Kim, and S.-W. Cheong, Phys. Rev. Lett. **94**, 087601 (2005).
[17] S. Lee *et al.*, Nature **451**, 805 (2008).
[18] O. Yamaguchi, H. Takemura, M. Yamashita, and A. Hayashida, J. Electrochem. Soc. **138**, 1492 (1991).
[19] Y. Mizoguchi, H. Onodera, H. Yamauchi, M. Kagawa, Y. Syono, and T. Hirai, Mater. Sci. Eng. A **217-218**, 164 (1996).
[20] A. A. Bossak, I. E. Graboy, O. Y. Gorbenko, A. R. Kaul, M. S. Kartavtseva, V. L. Svetchnikov, and H. W. Zandbergen, Chem. Mater. **16**, 1751 (2004).
[21] E. Magome, C. Moriyoshi, Y. Kuroiwa, A. Masuno, and H. Inoue, Jpn. J. Appl. Phys. **49**, 09ME06 (2010).
[22] H. Iida, T. Koizumi, and Y. Uesu, Phase Transitions **84**, 747 (2011).
[23] A. R. Akbashev, A. S. Semisalova, N. S. Perov, and A. R. Kaul, Appl. Phys. Lett. **99**, 122502 (2011).
[24] H. Iida, T. Koizumi, Y. Uesu, K. Kohn, N. Ikeda, S. Mori, R. Haumont, P.-E. Janolin, J-M. Kiat, M. Fukunaga, and Y. Noda, J. Phys. Soc. Jpn. **81**, 024719 (2012).
[25] Y. K. Jeong, J.-H. Lee, S.-J. Ahn, S.-W. Song, H. M. Jang, H. Chio, and J. F. Scott, J. Ame. Chem. Soc. **134**, 1450 (2012).
[26] Y. K. Jeong, J.-H. Lee, S.-J. Ahn, and H. M. Jang, Chem. Mat. **24**, 2426 (2012).
[27] L. J. Downie, R. J. Goff, W. Kockelmann, S. D. Forder, J. E. Parker, F. D. Morrison, and P. Lightfoot, J. Soli. Stat. Chem. **190**, 52 (2012).
[28] V. V. Pavlov, A. R. Akbashev, A. M. Kalashnikova, V. A. Rusakov, A. R. Kaul, M. Bayer, and R. V. Pisarev, J. Appl. Phys. **111**, 056105 (2012).
[29] W. Wang, J. Zhao, W. Wang, Z. Gai, N. Balke, M. Chi, H. N. Lee, W. Tian, L. Zhu, X. Cheng, D. J. Keavney, J. Yi, T. Z. Ward, Paul C. Snijders, H. M. Christen, W. Wu, J. Shen, and X. Xu, Phys. Rev. Lett. **110**, 237601 (2013).
[30] V. V. Roddatis, A. R. Akbashev, S. Lopatin, and A. R. Kaul, Appl. Phys. Lett. **103**, 112907 (2013).
[31] X. Xu and W. Wang, Modern Phys. Lett. B **28**, 1430008 (2014).
[32] R. L. White, J. Appl. Phys. **40**, 1061 (1969).
[33] M. Marezio, J. P. Remeika, and P. D. Dernier, Acta Crystallogr. B **26**, 2008 (1969).
[34] H. Wang, I. V. Solovyev, W. Wang, X. Wang, P. J. Ryan, D. J. Keavney, J.-W. Kim, T. Z. Ward, L. Zhu, J. Shen, X. M. Cheng, L. He, X. Xu, and X. Wu, Phys. Rev. B **90**, 014436 (2014).
[35] C. Xu, Y. Yang, S. Wang, W. Duan, B. Gu, and L. Bellaiche, Phys. Rev. B **89**, 205122 (2014).
[36] M. Fukunaga and Y. Noda, J. Phys. Soc. Jpn. **77**, 064706 (2008).
[37] T. Lonkai, D. G. Tomuta, U. Amann, J. Ihringer, R. W. A. Hendrikx, D. M. Többens, and J. A. Mydosh, Phys. Rev. B **69**, 134108 (2004).
[38] A. S. Gibbs, K. S. Knight, and P. Lightfoot, Phys. Rev. B **83**, 094111 (2011).
[39] K. Uusi-Esko, J. Malm, N. Imamura, H. Yamauchi, and M. Karppinen, Mater. Chem. Phys. **112**, 1029 (2008)
[40] M. Tanaka, M. Kato, N. Kimizuka, and K. Siratori, J. Phys. Soc. Jpn. **47**, 1737 (1979).
[41] M. Tanaka, K. Siratori, and N. Kimizuka, J. Phys. Soc. Jpn. **53**, 760 (1984).
[42] W. M. Reiff, I. E. Grey, A. Fan, Z. Eliezer, and H. Steinfink, J. Solid Sta. Chem. **13**, 32 (1975).
[43] C.-R. Lin, Y.-T. Tseng, S. G. Ovchinnikov, R. D. Ivantsov, I. S. Edelman, A. S. Fedorov, A. A. Kuzubov, D. A. Fedorov, S. S. Starchikov, and I. S. Lyubutin, Mat. Res. Exp. **1**, 025033 (2014).
[44] E. F. Bertaut, M. Mercier, and R. Pauthenet, J. Phys. **25**, 550 (1964).
[45] G. M. Nedlin, Sov. Phys. Solid State **6**, 2156 (1965).
[46] M. Fiebig, D. Fröhlich, K. Kohn, S. Leute, T. Lottermoser, V. V. Pavlov, and R. V. Pisarev, Phys. Rev. Lett. **84**, 5620 (2000).
[47] T. Lottermoser, M. Fiebig, D. Fröhlich, S. Leute, and K. Kohn, J. Magn. Mag. Mat. **226-30**, 1131 (2001).